Theor Chem Acc (2001) 106:369–378
DOI 10.1007/s002140100286

Theoretical
Chemistry Accounts

Regular article

Simultaneous calculation of Rydberg and valence excited states of formaldehyde

Thomas Müller, Hans Lischka

Institute for Theoretical Chemistry and Structural Biology, University of Vienna, Währingerstrasse 17, Vienna 1090, Austria

Received: 23 February 2001 / Accepted: 29 May 2001 / Published online: 11 October 2001

Abstract. The presence of low-lying Rydberg states interspersed among valence states constitutes a substantial challenge for the accurate quantum chemical calculation of electronically excited states because of the need to treat a relatively large number of states simultaneously. We present a general and efficient scheme that allows the treatment of a large number of Rydberg and valence states at the MR-CISD, MR-CISD + Q and MR-AQCC levels while using only a fraction of the size of the configuration space as compared to a full complete-active-space reference wave function. This scheme is applied to the calculation of vertical excitations and various avoided crossings between ten Rydberg and five valence singlet states of formaldehyde including transition dipole moments and oscillator strengths. Basis set effects, choice of configuration space and size-extensivity corrections have been considered. It is found that size-extensivity effects as computed by MR-CISD + Q and MR-AQCC play an important role especially for the description of the π–π^* state and for avoided crossings in which this state is involved.

Key words: Rydberg and valence states – Ab initio MR-CISD – Size-extensivity corrections – Transition moments – Potential-energy curves

1 Introduction

The quantum chemical calculation of electronically excited states is still a big challenge even for small molecules. One important reason for this fact is that frequently several low-lying Rydberg states are dispersed among valence states; therefore, even if only a few valence states are of interest, one is confronted – directly or indirectly – with the treatment of a relatively large number of states. Usually, for Rydberg states one main configuration dominates (single-reference character) and in many cases the interaction between Rydberg and valence configurations is small. In formaldehyde the situation is different: the experimental vacuum UV spectra [1, 2] show some unusually intense Rydberg series exhibiting large quantum defects, but no indication of the π–π^* valence state, even though the π–π^* excitation should be among the most intense ones.

A large number of quantum chemical calculations have been performed on excited states of formaldehyde, of which we mention the pioneering investigations by Whitten and Hackmeyer [3] and Buenker and Peyerimhoff [4] as well as more recent multireference configuration interaction (MR-CI) [5–9], complete-active-space perturbation theory to second order (CASPT2) [10] and equation-of-motion (EOM) calculations [11, 12]. The aforementioned puzzling experimental findings concerning irregularities in certain Rydberg series and the missing π–π^* state have been explained by Hachey et al. [6] in their MR double excitation CI (MRD-CI) calculations by interactions between Rydberg and valence states, associated in particular with the stretching coordinate of the CO bond. For vertical excitations, they found the π–π^* state, with 9.60 eV excitation energy, to be well above the n–π^* and σ–π^* valence and several Rydberg states. On stretching the CO bond, the π–π^* state is strongly stabilized and undergoes several avoided crossings with Rydberg states, causing intensity transfer to the latter and inhibiting thereby the detection of bands belonging to the π–π^* state. The spectroscopic identification of the σ–π^* state is still also uncertain. Similar to the π–π^* state it was shown that this state undergoes avoided crossings with Rydberg states as well [6].

Since a large number of electronic states and several sections of close approach between different potential-energy surfaces are to be calculated, special care has to be taken in order to achieve a proper balance between all these states in the quantum chemical calculations. Apart from the need for flexible and extended wave functions, questions concerning efficiency and economy of the calculation cannot be ignored either. In the MRD-CI calculations by Hachey et al. [6] one set of

Correspondence to: T. Müller or H. Lischka

self-consistent-field (SCF) molecular orbitals (MOs) computed for the n–π^* state was used for the CI expansion of both the Rydberg and the valence states. The bias connected with this particular choice of MOs had to be counterbalanced by means of extrapolations to full CI results. State-averaged multiconfigurational (MC) SCF calculations including all states of interest from the very beginning provide – in our opinion – a better balanced starting point. Such state-averaged MOs were used by Merchán and Roos [10] in their CASPT2 calculations on formaldehyde; however, these CASPT2 calculations were performed separately for states of different spatial symmetry with different active spaces for each symmetry, so there is no unique set of MOs for all states. Moreover, in these calculations a combined CAS was used both for valence and Rydberg orbitals. Thus, the computational effort increases rapidly with the number of Rydberg states to be calculated. Since Rydberg states are mostly of single-reference character, the use of CAS reference wave functions for their description is not required and much more compact wave functions should yield a similar quality of results at a drastically reduced computational cost.

For the proper description of avoided crossings and intersections of potential-energy surfaces (PES) for different electronic states, MR methods have to be applied. The MR-CI singles and doubles (MR-CISD) method [13, 14] is a very flexible and stable method for such tasks. The present work deals with a specific but still widely applicable wave function construction scheme within the MR-CISD approach, which is highly efficient for the present problem. We propose as a reference wave function a CAS wave function in the valence orbitals combined with a set of individual Rydberg configurations. Size-extensivity corrections are taken into account by the Davidson correction (MR-CISD + Q) [15] with its MR extension [16] and in a more consistent way by the MR-averaged quadratic coupled-cluster (MR-AQCC) approach [17, 18]. The latter is closely related to the MR-averaged coupled-pair functional (MR-ACPF) method [19]. The Davidson correction is straightforward to use and provides an a posteriori evaluation of size-extensivity corrections for the energy, but not for the wave function or properties. The MR-AQCC method has the advantage that size-extensivity effects are consistently built in from the very beginning. A level-shift method combined with root-following [20] is used for MR-AQCC calculations of excited states. Transition dipole moments and oscillator strengths are evaluated at the MR-CISD and MR-AQCC levels. For the latter method a linear-response-theory (LRT) approach (MR-AQCC/LRT) [20] has been developed, which allows reliable estimates of size-extensivity effects also for transition densities. The calculations are based on state-averaged MCSCF calculations with all states included in a single state-averaging procedure irrespective of their symmetry.

Our investigations aim at providing flexible and reliable methods for the calculation not only of energy surfaces but also for the evaluation of transition moment surfaces needed for the theoretical simulation of spectra and of the dynamics of photophysical and photochemical processes. Basis set effects, choice of reference configuration space and size-extensivity corrections are considered in order to verify the overall internal consistency of the results.

2 Computational details

The calculations were performed with atomic natural orbital basis sets [21] using spherical Gaussian-type orbitals. The basis set denoted as [431/21] contains a [4s3p1d] contracted basis set on carbon and oxygen and a [2s1p] contraction on H. Basis sets [542/32] and [5421/321] were constructed from [5s4p2d]/[3s2p] and [5s4p2d1f]/[3s2p1d] contracted basis sets, respectively. These valence-type basis sets were supplemented by one set of Rydberg orbitals [1s1p1d] with the exponents and contraction coefficients taken from Ref. [10]. The calculations were carried out at the experimental ground-state geometry ($R_{C-O} = 1.203$Å, $R_{C-H} = 1.101$Å, $\angle HCO = 121.9°$) [22]. The C_2 axis is aligned with the z-axis and the molecular plane coincides with the yz-plane of the coordinate system. In the calculations on the effect of C—O bond stretching the remaining internal coordinates were kept fixed at the ground state values.

The lowest five valence states [ground state (n^2), n–π^*, σ–π^*, π–π^* and n^2–π^{*2}] plus ten Rydberg states [n–($3s3p3d$) and π–$3s$] were computed. The orbital space for the MCSCF calculations was divided into doubly occupied (DOCC), CAS and auxiliary (AUX) sections. The DOCC and CAS orbitals were used for the description of the valence space, and the AUX orbitals represent the Rydberg orbitals. The DOCC orbitals were kept doubly occupied in all configuration state functions (CSFs) and in the CAS all possible CSFs were constructed. Three sets of CAS orbitals were selected. The first one (MINVAL) contains as active orbitals the $1b_2[\sigma(\mathrm{CH})], 5a_1[\sigma n(\mathrm{CO})], 1b_1(\pi), 2b_2[n_y(\mathrm{O})]$ and $2b_1(\pi^*)$ orbitals. For a qualitative description of MOs see, for example, Ref. [1]. Except for the $1b_2$ orbital, this is the minimal list of orbitals required for the description of the five valence states mentioned previously. The $1b_2$ orbital was added to improve the stability of the convergence of the MCSCF procedure and to alleviate intruder-state problems in the MR-AQCC calculations. In the second valence space (REDVAL) the strongly occupied $3a_1[\sigma(\mathrm{CO})]$ and $4a_1[\sigma(\mathrm{CH})]$ orbitals and the weakly occupied $6a_1[\sigma^*(\mathrm{CO})]$ orbital were added to the MINVAL space. The third choice is a valence CAS (VALENCE). Individual Rydberg configurations representing the $n-(3s, 3p, 3d)$ and π–$3s$ Rydberg states were constructed as single excitations from valence orbitals into AUX orbitals of type $(3a_1, 4a_1, 5a_1)^6(1b_1)^1(1b_2, 2b_2)^4(\mathrm{AUX})^1$ and $(3a_1, 4a_1, 5a_1)^6(1b_1)^2(1b_2, 2b_2)^3(\mathrm{AUX})^1$. Both $1b_2$ and $2b_2$ were treated equivalently in order to improve the MCSCF convergence. In this construction scheme only a fraction of the Rydberg configurations that would have been constructed via a standard restricted-active-space (RAS) SCF scheme (RAS1 empty, RAS2 = MINVAL-, REDVAL- or VALENCE-CAS, RAS3 = AUX) [23] was retained; hence, the computational cost is dominated by the size of the CAS space needed to accommodate the valence excitations, while the treatment of the Rydberg states requires little additional effort. The $(3s, 3p, 3d)$ Rydberg orbitals are classified according to symmetry as follows: $a_1 - 3s, 3p_z, 3d_{z^2}, 3d_{x^2-y^2}$; $b_1 - 3p_x, 3d_{xz}$; $b_2 - 3p_y, 3d_{yz}$; $a_2 - 3d_{xy}$. The orbital and CSF spaces are characterized by the number of orbitals per irreducible representation and by minimal and maximal orbital occupancies in Table 1. In the following, the shorthand notation σ is used for the $5a_1[\sigma n(\mathrm{CO})]$ orbital and n for the $2b_2[n_y(\mathrm{O})]$ orbital.

The number of states considered in the MCSCF state-averaging procedure was varied between 15 and 19 in different calculations in order to ascertain that all of the ten Rydberg and five valence states of interest were actually included in the MCSCF calculation. Single and double substitutions of reference-occupied orbitals by virtual ones created the total CSF expansion space for the MR-CISD and MR-AQCC calculations. Only the MINVAL and REDVAL reference spaces were considered. The carbon and oxygen 1s electrons were kept frozen. The calculations were carried out using the COLUMBUS program system [24–26] employing the atomic orbital integral package from DALTON [27]. In order to distinguish

Rydberg from valence-type orbitals and states, respectively, the spatial extent of the wave functions was characterized in terms of the expectation value, $\langle x^2 \rangle$, where x is the out-of-plane direction. The states are numbered in a standard order which corresponds to the ordering of states from the MR-CISD calculations given in Table 3.

The tremendous reduction in the size of the reference configuration space in our calculations with respect to a full CAS space is immediately apparent from the following comparison. The combined number of reference configurations for all four irreducible representations amounts to only 37 and 358 CSFs for the MINVAL and REDVAL spaces, respectively, with just 12 Rydberg configurations included. These numbers should be compared with the corresponding standard CAS and RAS approaches. The RASSCF choice described previously would include 375 and 9468 CSFs for MINVAL and REDVAL spaces, respectively. The CAS with eight electrons and 14 orbitals (MINVAL analogue) gives rise to about 273000 CSFs; the CAS with 12 electrons and 17 orbitals (REDVAL analogue) amounts to about 33 million CSFs.

Hence, we achieve a reduction of about 4–5 orders of magnitude with respect to the full CAS. These additional CSFs included in the full CAS are all higher excitations from valence orbitals into Rydberg orbitals and can be left out of the reference wave function without any significant loss in accuracy, as the MR-CISD and MR-AQCC results presented later will show. The full CAS reference spaces are only tractable with internal contraction schemes as used, for example, in the CASPT2 method [28], but even there practical limits in terms of the number of active orbitals are encountered soon.

Table 1. Characterization of multiconfigurational self-consistent-field (*MCSCF*) orbital and configuration spaces

Orbital space	Range of occupation numbers	a_1	b_1	b_2	a_2
	MINVAL				
DOCC	8	4	0	0	0
CAS	7–8	1	2	2	0
AUX[a]	0–1	4	2	2	1
	REDVAL				
DOCC	4	2	0	0	0
CAS	11–12	4	2	2	0
AUX[a]	0–1	4	2	2	1
	VALENCE				
DOCC	4	2	0	0	0
CAS	11–12	5	2	3	0
AUX[a]	0–1	4	2	2	1
Number of averaged states		A_1	B_1	B_2	A_2
MINVAL		5	3	4	3
REDVAL		5	3	4	4
VALENCE		5	4	6	4

[a] Excitations into the AUX space of type $(3a_1, 4a_1, 5a_1)^6(1b_1)^1(1b_2, 2b_2)^4(\mathrm{AUX})^1$ and $(3a_1, 4a_1, 5a_1)^6(1b_1)^2(1b_2, 2b_2)^3(\mathrm{AUX})^1$, only

3 Results and discussion

The main purpose of the MCSCF calculations is to provide adequate orbitals for the subsequent MR-CISD and MR-AQCC calculations. The principal criteria for judging the quality of the MCSCF calculations are the requirements that the CSF expansion at the MCSCF level represents the character of the excited states correctly and that the MOs have the desired valence or Rydberg character according to Table 1. If these two requirements are met, the balance of excitation energies will be taken care of by the post-MCSCF method MR-CISD, MR-CISD + Q or MR-AQCC. MCSCF results for the MINVAL, REDVAL and VALENCE reference spaces (for definition see Table 1) and the [431/21] basis can be found in Table 2. With increasing size of the configuration space from MINVAL to VALENCE, the excitation energy of the π–π^* state is reduced drastically by about 1.4 eV and the ordering of the n^2–π^{*2} and π–π^* states is reversed; however, the π–π^* state is still located at too high excitation energy in comparison to

Table 2. Configuration-space dependence of vertical excitation energies, E_{exc} (eV), and spatial extent, $\langle x^2 \rangle$ (au), at the MCSCF level ([431/21] basis set at experimental ground-state geometry)

State[a]	MINVAL		REDVAL		VALENCE	
	E_{exc}	$\langle x^2 \rangle$	E_{exc}	$\langle x^2 \rangle$	E_{exc}	$\langle x^2 \rangle$
E_{tot}[b]	−113.903432		−113.943589		−114.002156	
$^1A_1(n^2)$	0.00	8.81	0.00	8.67	0.00	8.64
$^1A_2(n$–$\pi^*)$	3.34	10.67	3.65	10.59	3.85	10.37
$^1B_2(n$–$3s)$	6.24	23.07	7.32	22.17	9.66	23.80
$^1B_2(n$–$3p_z)$	7.09	23.21	8.17	23.26	12.24	22.04
$^1A_1(n$–$3p_y)$	7.08	19.74	8.17	19.74	9.53	18.90
$^1A_2(n$–$3p_x)$	7.33	47.87	8.41	47.59	9.91	47.34
$^1B_2(n$–$3d_{x^2-y^2})$	8.01	50.72	9.10	51.19	10.61	52.30
$^1B_1(n$–$3d_{xy})$	8.10	58.30	9.18	55.44	10.71	58.22
$^1B_2(n$–$3d_{z^2})$	8.17	39.46	9.26	38.53	10.79	38.66
$^1A_1(n$–$3d_{yz})$	8.20	25.25	9.23	24.33	11.02	21.20
$^1A_2(n$–$3d_{xz})$	8.25	62.16	9.34	62.10	10.87	61.81
$^1B_1(\sigma$–$\pi^*)$	8.85	11.15	9.26	13.62	9.82	10.22
$^1A_1(\pi$–$\pi^*)$	11.73	9.54	10.88	10.38	10.31	13.30
$^1A_1(n^2$–$\pi^{*2})$	10.29	14.12	10.28	13.47	11.58	12.15
$^1B_1(\pi$–$3s)$	9.10	22.65	10.21	22.54	12.72	24.25

[a] Dominant configuration in parentheses
[b] Ground-state energy in hartree

post-MCSCF results (see later). This is an indication for the particular importance of dynamic electron correlation for the π–π^* state. In going from the MINVAL to the VALENCE space only the valence part of the active orbital space is extended and, thus, the description of the valence states and in particular of the ground state is improved. As the ground-state energy is decreased by about 2.7 eV (MINVAL versus VALENCE), the Rydberg states are shifted by roughly the same amount to higher excitation energies. The excitation energies of the Rydberg states computed with the MINVAL space are significantly too small compared to post-MCSCF results. With the REDVAL space the situation appears to be better balanced. Further extension of the CAS reverses the bias.

Despite the large changes in excitation energies with respect to different MCSCF calculations, the character of the total wave function (see $\langle x^2 \rangle$ values in Table 2) and that of individual MOs remains practically unchanged. The first two states of $^1B_1$ symmetry are an exception since they approach each other energetically in the REDVAL calculations. The small variations of the MOs computed with different MCSCF configuration spaces demonstrate that they are all well suited for subsequent MR-CISD and MR-AQCC calculations. The errors in the excitation energies are due to missing dynamical electron correlation and will be corrected by the MR-CISD and related methods. In particular, the largely overestimated MCSCF excitation energy for the π–π^* state arises mainly from deficiencies in the configuration space and not – as in the case of ethylene (see Ref. [29] and references therein) – from the choice of inadequate molecular orbitals.

The vertical excitation energies and $\langle x^2 \rangle$ values are displayed for the MR-CISD, MR-SDCI + Q, MR-AQCC and MR-AQCC/LRT calculations based on the MINVAL reference space and the [431/21] basis set in Table 3. Incorporating dynamical electron correlation through MR-CISD improves the balance of all states substantially in comparison to the previously reported MCSCF results (Table 2). The order of the 4^1A_1 and 5^1A_1 states is reversed with respect to MCSCF and the excitation energy for the π–π^* state is reduced by about 1.6 eV. The Davidson correction for the excitation energies amounts in most cases to about 0.15 eV. Not unexpectedly, it is largest (0.35 eV) for the π–π^* excitation. A shift of similar size is observed for the π–3*s* excitation which is derived from a doubly excited configuration in the valence space not included in the reference space. The MR-AQCC and MR-AQCC/LRT results are in line with those from MR-CISD + Q; however, as MR-CISD + Q tends to slightly overestimate the size-extensivity correction, a slightly different energetic ordering of neighboring states results ($3\ ^1A_1, 1-2\ ^1B_1, 4\ ^1B_2, 3\ ^1A_2$). Moreover, MR-CISD predicts a predominantly valence character for the 4^1A_1 state with strong mixing of π–π^* and n^2–π^{*2} configurations, whereas MR-AQCC and MR-AQCC/LRT indicate interaction between Rydberg and π–π^* configurations. Since the basis set choice eliminates higher members of the *n*-Rydberg series we cannot rule out the omission of interactions between the π–π^* state and suppressed members of the *n*-Rydberg series; however, Hachey et al. [6] included up to 5d members of the *n*-Rydberg series and also reported (π–π^*)-(n^2–π^{*2}) configuration mixing at the MR-DCI level of theory.

MR-AQCC/LRT differs from MR-AQCC only by the fact that the state-specific diagonal shift for external configurations [20] is replaced by the ground-state shift. This furnishes a reasonable approximation provided the reference configuration space is sufficiently large and the correlation energy due to dynamical electron correlation is of similar size for all states; however, for the Rydberg states the electron correlation energy is smaller in absolute value than for valence states. Thus, using the ground-state shift for the Rydberg states overemphasizes somewhat the size-extensivity effects for those states; therefore, the MR-AQCC/LRT Rydberg excitation energies are systematically smaller (about 0.1 eV) than the MR-AQCC values. For valence states the respective differences are about 0.05 eV. With respect to the spatial extent of the molecular wavefunction we note substantial differences between MR-CISD and MR-AQCC results for the lowest states of B_1 symmetry arising from their near degeneracy at the MR-AQCC level.

MR-CISD and MR-CISD + Q vertical excitation energies and $\langle x^2 \rangle$ values for calculations based on the REDVAL space and the [431/21] basis are shown in Table 4. As expected, the size of the Davidson corrections is significantly reduced and amounts for the majority of states to less than 0.05 eV. Since the MR-CISD + Q excitation energies obtained from the MINVAL and REDVAL calculations are very close to each other we conclude that size-extensivity-corrected data at the MINVAL level are sufficient in order to achieve an internal consistency with respect to the size of the configuration space of better than 0.1 eV.

The basis set effects for excitation energies are presented in Table 5 at the MR-CISD + Q level and for the MINVAL reference configuration space. Between basis sets [431/21] and [542/32] we note only a small, unsystematic shift of up to 0.1 eV for excitation energies. Enlarging the basis set size by additional f functions on C and O and by d functions on H (basis [5421/321]) mainly gives rise to an improved description of the valence excited states. The excitation energies of the Rydberg states increase thereby by at most 0.1 eV. This indicates that the basis-set-related accuracy of about 0.1 eV for excitation energies has already been achieved with the [431/21] basis set.

In general we find very good agreement of the calculated results with available experimental data (Table 3). Such comparisons have to be regarded sometimes with caution since computed vertical excitation energies do not have a directly observable experimental counterpart. We reconfirm the finding that the vertically excited n–$3p_z$ state is lower in energy than the n–$3p_y$ state, a fact first observed by Yeager and McKoy [11] and Harding and Goddard [5] and reemphasized by Hachey et al. [6]. At the MR-CISD and MR-CISD + Q levels using the MINVAL reference space and the [431/21] basis set, the energetic splitting of these two states is rather small (Table 3). The two MR-AQCC methods reproduce the experimental splitting better. However,

Table 3. E_{exc} (eV) and $\langle x^2 \rangle$ and $\langle r^2 \rangle$ (au) based on MR-CISD, MR-CISD + Q, MR-AQCC and MR-AQCC/LRT calculations using the MINVAL space ([431/21] basis set at experimental ground state geometry)

State[d]	CI		CI + Q	AQCC		LRT		exp.	EOM-CCSD[a]		CASPT2[b]	MR-CI[c]
	E_{exc}	$\langle x^2 \rangle$	E_{exc}	E_{exc}	$\langle x^2 \rangle$	E_{exc}	$\langle x^2 \rangle$	E_{exc}	E_{exc}	$\langle r^2 \rangle$	E_{exc}	E_{exc}
E_{tot}[e]	−114.239774		−114.275610	−114.268601		−114.268601						
$1\ ^1A_1(n^2)$	0.00	8.81	0.00	0.00	8.86	0.00	8.86	0.00	0.00	20.6	0.00	0.00
$1\ ^1A_2\ (n–\pi^*)$	3.93	10.57	4.07	4.04	10.48	3.98	10.47	3.79[f]	3.98	20.9	3.91	4.05
$1\ ^1B_2\ (n–3s)$	7.11	22.28	7.27	7.21	21.80	7.12	21.81	7.09[g]	6.99	30.7	7.30	7.15
$2\ ^1B_2\ (n–3p_z)$	7.97	22.85	8.10	8.03	21.58	7.94	21.25	7.98[g,h]	7.93	29.5	8.09	8.05
$2\ ^1A_1(n–3p_y)$	7.98	19.59	8.13	8.24	19.27	8.16	19.11	8.13[g,h]	7.99	33.9	8.12	8.10
$2\ ^1A_2(n–3p_x)$	8.21	47.29	8.34	8.46	45.58	8.38	44.97	8.37[i]	8.45	30.8	8.32	8.32
$3\ ^1B_2\ (n–3d_{x^2-y^2})$	8.98	47.71	9.15	9.09	45.24	8.99	44.88		9.25	31.1	9.13	9.05
$1\ ^1B_1\ (n–3d_{xy})$	9.09	58.04	9.26	9.37	55.68	9.29	46.10		9.84	30.3	9.23	9.32
$4\ ^1B_2(n–3d_{z^2})$	9.15	42.43	9.30	9.24	44.60	9.14	44.68		9.98	30.1	9.31	9.25
$3\ ^1A_1(n–3d_{yz})$	9.14	24.40	9.28	9.38	22.43	9.29	21.38		10.16	34.5	9.24	9.25
$3\ ^1A_2(n–3d_{xz})$	9.21	61.93	9.36	9.49	61.61	9.41	61.52	9.22[h]	10.67	30.3	9.31	9.34
$2\ ^1B_1(\sigma–\pi^*)$	9.33	10.96	9.40	9.37	16.48	9.32	23.05		9.33	20.9	9.09	9.35
$4\ ^1A_1(\pi–\pi^*)$	10.15	12.35	9.80	9.84	17.37	9.83	16.72		9.47	28.0	9.77	9.60
$5\ ^1A_1(n^2–\pi^{*2})$	10.63	12.84	10.54	–	–	10.58	13.64					
$3\ ^1B_1(\pi–3s)$	10.64	22.07	11.00	10.96	21.09	10.84	20.63					10.66

[a] Ref. [12]
[b] Ref. [10]
[c] Ref. [6]
[d] Dominant configuration in parentheses
[e] Ground-state energy in hartree
[f] Ref. [34]
[g] Ref. [2]
[h] Experimental $n–3p_y$ and $n–3p_z$ assignments interchanged
[i] Ref. [35]

with increasing basis set size and configuration space MR-CISD + Q approaches the experimental splitting as well. In view of the uniformness of our results, the n–3d Rydberg excitation energies are surprisingly different from the experimentally assigned value (band orign of 8.88 eV) [30]. This finding is shared by other recent high-level ab initio calculations [6, 10]. Their vertical excitation energies and $\langle x^2 \rangle$ values are in good agreement with our data; however, EOM-CC [12] predicts much too high excitation energies for the n–3d Rydberg states (e.g. a deviation of 1.3 eV for the n–3d_{xz} state) and, correspondingly, a different energetic ordering of Rydberg and valence states. The reported EOM-CC-based $\langle r^2 \rangle$ values for the Rydberg states fall short by a factor of 2 and more, which suggests that the aforementioned deviations may be related to the basis set choice. Considering the good agreement of theoretical work based upon different methods, our n–3d vertical excitation energies indirectly support the reassignment of the experimental n–3d data of Hachey and coworkers [7, 9]. Owing to this uncertainty of the experimental assignment, the experimental n–3d oscillator strengths are excluded in the subsequent discussion of transition moments.

Table 4. E_{exc} (eV) and $\langle x^2 \rangle$ (au) based on MR-CISD and MR-CISD + Q calculations using the REDVAL reference space ([431/21] basis set at experimental ground-state geometry)

State	CI		CI + Q
	E_{exc}	$\langle x^2 \rangle$	E_{exc}
1 $^1A_1(n^2)$	0.00	8.80	0.00
$1^1A_2(n–\pi^*)$	4.00	10.54	4.09
1 $^1B_2(n–3s)$	7.27	22.07	7.23
2 $^1B_2(n–3p_z)$	8.13	22.58	8.05
2 $^1A_1(n–3p_y)$	8.18	19.56	8.14
2 $^1A_2(n–3p_x)$	8.41	46.98	8.36
3 $^1B_2(n–3d_{x^2-y^2})$	9.16	47.64	9.14
$1^1B_1(n–3d_{xy})$	9.27	57.25	9.24
4 $^1B_2(n–3d_{z^2})$	9.33	42.15	9.28
3 $^1A_1(n–3d_{yz})$	9.32	23.15	9.29
3 $^1A_2(n–3d_{xz})$	9.42	61.88	9.39
2 $^1B_1(\sigma–\pi^*)$	9.37	11.61	9.41
4 $^1A_1(\pi–\pi^*)$	10.03	12.83	9.72
5^1A_1 $(n^0–\pi^{*2})$	10.59	12.93	10.59
3 $^1B_1(\pi–3s)$	10.91	21.59	11.13

Of particular importance for the analysis of electronic spectra are the interactions of potential-energy curves due to avoided crossings and related changes in oscillator strengths and transition dipole moments. The main coordinate of interest is the CO bond distance, to which – following the work of Hachey et al. [6] – our investigations were restricted. Potential-energy curves computed by the MR-CISD, MR-CISD + Q and MR-AQCC/LRT methods are displayed in Fig. 1. Only the excited states of A_1 and B_1 symmetry are considered as among these states avoided crossings between the σ–π^* and π–π^* valence states and Rydberg states along extension of the CO bond distance are found. There are three major interactions between the A_1 states and two between the B_1 states. The positions of these avoided crossings depend significantly on the method, the basis set and the configuration space. They are shifted by about 0.05 Å to shorter CO bond distances when going from MR-CISD to MR-CISD + Q to MR-AQCC/LRT.

On passing through an avoided crossing, the changes in character of the participating states can be viewed by means of the $\langle x^2 \rangle$ values. Their dependence on the CO bond distance for all the states investigated is displayed in Fig. 2. Most of the avoided crossings are associated with a very rapid change in the character of the state ($1^1B_1/2^1B_1$, $2^1B_1/3^1B_1$, $2^1A_1/3^1A_1$, $4^1A_1/5^1A_1$). In contrast, the $3^1A_1/4^1A_1$ avoided crossing is much smoother and takes place over a considerable range of bond distance. This suggests that except for the latter case the interactions between the Rydberg and the valence configurations considered here are associated with a relatively small interaction matrix element.

Table 5. Basis set dependence of E_{exc} (eV), and $\langle x^2 \rangle$ (au), at MR-CISD + Q level using the MINVAL reference space ([43-1/21] basis set at experimental ground-state geometry)

Basis State[a]	[431/21]		[542/32]		[5421/321]	
	E_{exc}	$\langle x^2 \rangle$[c]	E_{exc}	$\langle x^2 \rangle$[c]	E_{exc}	$\langle x^2 \rangle$[c]
E_{tot}[b]	−114.275610		−114.302433		−114.3396982	
1 $^1A_1$	0.00	8.81	0.00	8.71	0.00	8.69
1 $^1A_2(n–\pi^*)$	4.07	10.57	4.04	10.53	4.03	10.47
1 $^1B_2(n–3s)$	7.27	22.28	7.19	19.50	7.28	19.36
2 $^1B_2(n–3p_z)$	8.10	22.85	8.03	20.71	8.12	20.54
2 $^1A_1(n–3p_y)$	8.13	19.59	8.10	18.49	8.19	18.48
2 $^1A_2(n–3p_z)$	8.34	47.29	8.33	48.40	8.43	48.43
3 $^1B_2$ $(n–3d_{x^2-y^2})$	9.15	47.71	9.08	51.60	9.17	52.23
1 $^1B_1$ $(n–3d_{xy})$	9.26	58.04	9.26	57.40	9.35	56.31
4 $^1B_2(n–3d_{z^2})$	9.30	42.42	9.28	39.18	9.38	38.60
3 $^1A_1(n–3d_{yz})$	9.28	24.40	9.27	24.51	9.35	24.24
$3^1A_2(n–3d_{xz})$	9.36	61.93	9.36	63.97	9.45	63.93
2 $^1B_1(\sigma–\pi^*)$	9.40	10.96	9.38	10.89	9.32	11.97
4 $^1A_1(\pi–\pi^*)$	9.80	12.35	9.73	12.27	9.73	12.48
5 $^1A_1(n^0–\pi^{*2})$	10.54	12.85	10.45	12.74	10.39	12.59
3 $^1B_1(\pi–3s)$	11.00	22.07	10.90	19.17	10.94	19.03

[a] Dominant configuration in parentheses
[b] Ground-state energy in hartree
[c] Derived from the corresponding MR-CISD calculations

The $1^1B_1/2^1B_1$ avoided crossing is located in the region of the vertical excitation. This has an important effect on the extrapolations of energies and properties with respect to the basis set limit and/or full CI (FCI). Changing the basis set or the configuration space results in moving the location of the avoided crossing or equivalently moving on the PES relative to these critical points. Energy and property changes close to these regions may be large and cannot be solely attributed to direct basis set or configuration space effects. Such a situation is, for example, encountered for the vertical excitations computed for the n–$3d_{xy}$ and σ–π^* $^1B_1$ states. As one can see from Fig. 1, these two states exhibit an avoided crossing very close to the CO distance of the ground state. As is shown in Table 5, increasing the size of the basis set reverses the ordering of the n–$3d_{xy}$ and σ–π^* $^1B_1$ states in the [5421/321] basis as compared to [542/32]. This coupling of the location of the avoided crossing on the basis sets and the choice of the wave function prohibits straightforward extrapolations of excitation energies and FCI limits.

It is interesting to note that within several sections of the potential-energy curves the B_1 and A_1 states almost lie (method-dependent) on top of each other. This is not unexpected for different members of the n–$3d$ series [$1^1B_1, 3^1A_1$ at 1.15–1.20 Å; $2^1B_1, 4^1A_1$ at 1.25–1.35 Å (MR-CISD + Q)] because of their small energetic splitting. A similar close following is observed for the $2^1A_1(\pi$–$\pi^*)$ and $^1B_1(\sigma$–$\pi^*)$ states (see the MR-CISD + Q and MR-AQCC potential-energy curves at CO distances greater than 1.30 Å). It has been shown recently [31] that the energy surfaces of these states exhibit a conical intersection (not shown in Fig. 1) at a CO distance of about 1.5 Å.

The potential-energy curves computed in this work (Fig. 1) agree qualitatively quite well with those reported by Hachey and coworkers [6, 8]; however, we find that the potential-energy curves participating in an avoided crossing approach each other much closer in our calculations. It is expected that these avoided crossings will turn into true crossings on variation of the remaining geometry parameters. It is interesting to note that similar potential-energy curves were computed for a cut along the CO bond of acetone using the CASPT2 [32] and the time-dependent density functional theory [33] approaches, respectively.

The oscillator strengths and the magnitude of the transition dipole moment vector (μ_{tr}, transition dipole length) for vertical transitions computed at the MCSCF, MR-CISD and MR-AQCC/LRT levels are collected in Table 6. For MR-CISD, the oscillator strength is calculated in two different ways: using MR-CISD transition moments and MR-CISD excitation energies (f) and using MR-CISD transition moments and the more reliable MR-CISD + Q excitation energies (f_Q). Large differences between MCSCF results and those obtained with MR-CISD and MR-AQCC/LRT are observed in

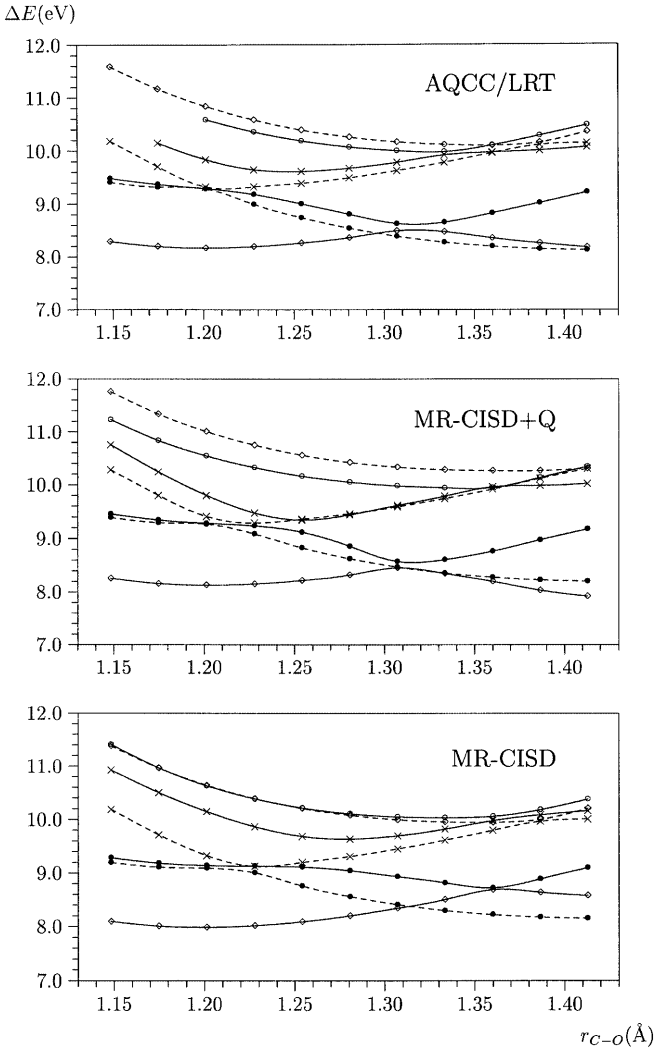

Fig. 1. Potential energy curves of A_1 states (solid: $2A_1$ (◇), $3A_1$ (●), $4A_1$ (×), $5A_1$ (○)) and B_1 states (dashed: $1B_1$ (●), $2B_1$ (×), $3B_1$ (◇)) as a function of the C—O bond distance. The energy is given relative to the minimum energy of the ground state

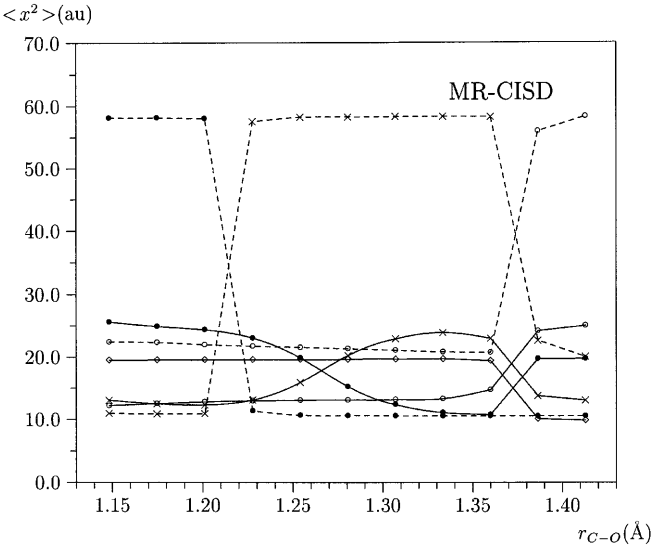

Fig. 2. $\langle x^2 \rangle$ curves of A_1 states (solid: $2A_1$ (◇), $3A_1$ (●), $4A_1$ (×), $5A_1$ (○)) and B_1 states (dashed: $1B_1$ (●), $2B_1$ (×), $3B_1$ (◇)) as a function of the C—O bond distance

Table 6. Oscillator strengths, f, f_Q, and the magnitude of the transition dipole moment vector, μ_{tr} (au), for optically allowed vertical transitions from the ground state using the MINVAL reference space ([431/21] basis set at experimental ground-state geometry)

Transition	MCSCF		CI			LRT		CASSCF[a]	MR-DCI[b]	GVB-CI[c]	EOM	
	f	μ_{tr}	f	μ_{tr}	f_Q[d]	f	μ_{tr}	f	f	f	f[e]	f[f]
$1\ ^1B_2(n\text{–}3s)$[g]	0.008	0.227	0.018	0.318	0.018	0.018	0.323	0.006	0.005	0.006	0.02	0.022
$2\ ^1B_2(n\text{–}3p_z)$[g]	0.028	0.403	0.032	0.402	0.032	0.040	0.455	0.023	0.021	0.015	0.04	0.042
$2\ ^1A_1(n\text{–}3p_y)$[g]	0.029	0.410	0.039	0.448	0.040	0.043	0.465	0.041	0.039	0.030	0.05	0.057
$3\ ^1B_2(n\text{–}3d_{x^2-y^2})$	0.003	0.120	0.008	0.193	0.008	0.010	0.212	0.006	–	–	–	0.042
$1\ ^1B_1(n\text{–}3d_{xy})$	0.000	0.011	0.001	0.054	0.001	0.000	0.044	0.000	–	0.000	–	0.002
$4\ ^1B_2(n\text{–}3d_{z^2})$	0.003	0.112	0.001	0.071	0.001	0.000	0.027	0.001	–	0.000	–	0.000
$3\ ^1A_1(n\text{–}3d_{yz})$	0.008	0.197	0.009	0.195	0.009	0.018	0.282	0.003	0.005	0.000	–	0.069
$2\ ^1B_1(\sigma\text{–}\pi^*)$	0.004	0.129	0.002	0.092	0.002	0.000	0.030	0.012	–	–	0.002	0.001
$4\ ^1A_1(\pi\text{–}\pi^*)$	0.489	1.303	0.163	0.810	0.158	0.100	0.646	0.277	–	–	0.10	0.063
$5\ ^1A_1(n^2\text{–}\pi^{*2})$	0.005	0.134	0.081	0.557	0.080	0.007	0.160	–	–	–	–	–
$3\ ^1B_1(\pi\text{–}3s)$	0.077	0.587	0.048	0.427	0.049	0.044	0.409	–	–	–	–	–

[a] Ref. [10]
[b] Ref. [8]
[c] Ref. [5]
[d] For definition, see text
[e] Ref. [11]
[f] Ref. [12]
[g] Experimental oscillator strengths: 0.032 (n–$3s$), 0.019 (n–$3p_z$), 0.036 (n–$3p_y$) [36]. The experimental assignments of n–$3p_y$ and n–$3p_z$ states were interchanged

many cases. This reflects the importance of dynamical electron correlation. The MR-AQCC/LRT transition dipole lengths as well as oscillator strengths differ in several cases substantially from those obtained by the MR-CISD method, i.e. π–π^*, n–$3d_{yz}$, σ–π^* and n–$3d_{xy}$. All these deviations are connected with two avoided crossings near the equilibrium geometry as already discussed.

Experimentally, the n–$3s$ excitation is of similar intensity as the the n–$3p_y$ excitation and about twice of that for the n–$3p_z$ Rydberg state (Table 6). We find, however, that the n–$3p_y$ and n–$3p_z$ transitions are of similar intensity and more intense than the n–$3s$ excitation. This observation is shared by previously reported theoretical data [5, 8, 11, 12]. Whereas the EOM-based data [11, 12] for these three states are in acceptable agreement with our MR-CISD and MR-AQCC/LRT oscillater strengths, the MR-DCI [8] and the generalized valence bond CI [5] method predict weaker transition intensities, especially for the n–$3s$ excitation. On the other hand, the reported oscillator strengths for the n–$3d$ excitations from EOM calculations [12] are by up to 4 times larger than those derived from CI methods. This is probably related to the erratic behavior of the EOM excitation energies and spatial extent of the n–$3d$ Rydberg states (see earlier). The CASSCF oscillator strengths reported by Merchán and Roos [10] differ unsystematically from our MCSCF data. This appears quite reasonable considering the widely different configuration spaces and the state-averaging procedure. We also note that the π–$3s$ transition is predicted to be fairly intense although no such excitation is observed experimentally. However, the basis set choice eliminates higher members of the n-Rydberg series, which according to an empirical estimate [6] may be expected to interact with the π–$3s$ state, distributing its intensity over a considerable number of states.

Dynamical electron correlation effects play an important role for the calculation of oscillator strengths and transition moments. Moreover, size-extensivity corrections have a sizeable impact on the results even in cases which are not associated with a near avoided crossing of states. On comparing the oscillator strengths based on MR-CISD (f_Q) and MR-AQCC(LRT) (Table 6) we note large differences for states with nearby avoided crossings (such as the 3–5 $^1A_1$ states). Since f_Q is calculated from the MR-CISD + Q energy and the MR-CISD transition moment, it does not take into account relaxation of the wave function in the presence of size-extensivity corrections. The comparison of MR-CISD- and MR-AQCC/LRT-based transition dipole lengths indicates that regions close to avoided crossings give rise to substantial changes in the transition dipole length; hence, in these critical regions the energy and the transition moments should be evaluated on the same theoretical grounds, i.e. no extrapolation of one quantity without consistent extrapolation of the other quantity.

The dependence of the transition dipole length on the CO bond distance for excitations from the ground state to the excited states of A_1, B_1 and B_2 symmetry are displayed in Fig. 3. The transition with the highest transition dipole length corresponds to the π–π^* excitation throughout. The π–π^* state starts as the 5^1A_1 state on the left-hand side of Fig. 3 (MR-CISD results), switches to 4^1A_1 at about 1.17 Å, to 3^1A_1 at about 1.27 Å and to 2^1A_1 at about 1.37 Å. The avoided crossing between the 1^1B_1 and 2^1B_1 states at about 1.21 Å (Figs. 1, 2) finds its counterpart in the crossing of the respective curves at around 1.22 Å in Fig. 3. A relatively large change in the transition dipole moment also occurs for the avoided crossing between potential-energy curves for the $2\ ^1B_1(n\text{–}3d_{xy})$ and $3\ ^1B_1(\pi\text{–}3s)$ at around 1.38 Å. Similar behavior is observed for the MR-AQCC/LRT curves. In this case, the crossing points for the transition

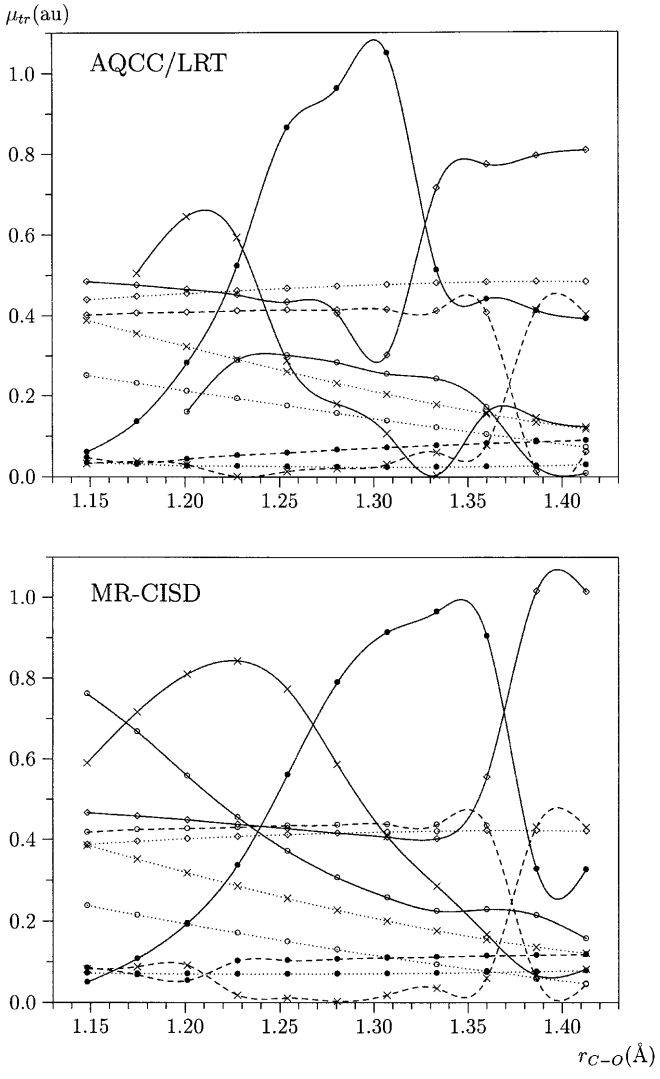

Fig. 3. Transition dipole length curves, μ_{tr}, for excitations from the ground state to A_1 states (solid: $2A_1$ (◇), $3A_1$ (●), $4A_1$ (×), $5A_1$ (○)), B_1 states (dashed: $1B_1$ (●), $2B_1$ (×), $3B_1$ (◇)) and B_2 states (dots: $1B_2$ (×), $2B_2$ (◇), $3B_2$ (○), $4B_2$ (●)) as a function of the C—O bond distance

dipole length curves are shifted somewhat – in agreement with the changes in the potential-energy curves given in Fig. 1 – to smaller CO bond lengths. In contrast to the strong variations related to the avoided crossings by the π–π^* state, a very regular behavior of the geometry dependence of μ_{tr} is observed for other Rydberg transitions. This is illustrated by the excitations to the B_2 states, which display a completely smooth and essentially linear dependence on the CO bond length.

4 Conclusions

A general scheme was presented that allows the simultaneous treatment of a large number of Rydberg and valence states within the MR-CISD/MR-AQCC approach using only a fraction of the size of the configuration space as compared to a full CAS reference space. The active orbitals for the reference configurations are divided into a CAS part for the valence orbitals and into an AUX one for the Rydberg orbitals. The concomitant reduction in the size of the configuration space is especially crucial for an uncontracted MR-CISD approach. Beyond the Davidson approximation, size-extensivity effects were computed within the MR-AQCC and MR-AQCC/LRT approaches. Because of the consistent inclusion of size-extensivity contributions into the MR-AQCC method, transition moments and oscillator strengths could be calculated at this level as well. This scheme was applied to vertical valence and Rydberg excitations and to the difficult case of various avoided crossings between Rydberg and valence excited states of formaldehyde. An internal consistency of vertical excitation energies with respect to basis set effects and extension of the active valence space of roughly 0.1 eV was achieved. An investigation of size-extensivity effects was carried out for vertical excitations and for cuts through the PES along the CO bond using MR-CISD, MR-CISD + Q and MR-AQCC/LRT. Most notable is the size-extensivity correction for the excitation to the π–π^* state of 0.3 eV (MINVAL reference space), whereas it is only 0.15 eV for Rydberg states. This trend persists even in the larger (REDVAL) reference space. Quite generally, we find that the MRCISD + Q and MR-AQCC/LRT methods produce quite similar potential-energy curves and that the MR-CISD curves deviate considerably. This may be taken as an indication that although MR-CISD is, owing to its robustness, very well suited for PES calculations, it can contain undesirable artifacts (as for the π–π^* state in this case), even for relatively large expansion sets of configuration functions. The locations of the avoided crossings are very sensitive to basis set and size-extensivity effects. For the extrapolation of energies or properties to the basis set limit and/or to FCI one has to ensure that no state of interest comes close to regions of avoided crossings. Apart from standard basis set effects known from calculations on well-separated states, additional effects arise because basis set changes correspond to movements on the PES relative to the location of the avoided crossing associated with potentially rapid changes of the observable.

The potential-energy curves are in qualitative agreement with those of Hachey et al. [6], but we find that the potential-energy curves for states participating in the avoided crossings approach each other much more closely than shown in Ref. [6]. Thus, we expect that on further geometry variations these avoided crossing will turn into conical intersections.

The computed oscillator strengths and transition dipole moments are largely affected by dynamical electron correlation as well as size-extensivity corrections. Our MR-AQCC/LRT results indicate that in particular near avoided crossings the relaxation of the wave function in the presence of size-extensivity corrections is nonnegligible.

Acknowledgements. This work was performed under the auspices of the Austrian Science Fund within the framework of the Special Research Program F16, project no. P12778-CHE, and of COST/D9, project no. D9/0006/98.

References

1. Moule DC, Walsh AD (1975) Chem Rev 75: 67
2. Brint P, Connerade JP, Mayhew C, Sommer K (1985) J Chem Soc Faraday Trans 281: 1643
3. Whitten JL, Hackmeyer M (1969) J Chem Phys 51: 5584
4. Buenker RJ, Peyerimhoff SD (1970) J Chem Phys 53: 1368
5. Harding LB, Goddard WA III (1977) J Am Chem Soc 99: 677
6. Hachey MRJ, Bruna PJ, Grein F (1995) J Phys Chem 99: 8050
7. Hachey MRJ, Grein F (1996) Chem Phys Lett 256: 179
8. Grein F, Hachey MRJ (1996) Int J Quantum Chem S30: 1661
9. Perić M, Grein F, Hachey MRJ (2000) J Chem Phys 113: 9011
10. Merchán M, Roos BO (1995) Theor Chim Acta 92: 227
11. Yeager DL, McKoy V (1974) J Chem Phys 60: 2714
12. Gwaltney SR, Barlett RJ (1995) Chem Phys Lett 241: 26
13. Shavitt I (1977) In: Schaeffer HF III (ed) Methods of electronic structure theory. Plenum, New York, p 189
14. Shavitt I (1998) Mol Phys 94: 3
15. Davidson ER (1974) In: Daudel R, Pullman B (eds) The world of quantum chemistry. Reidel, Dodrecht, p 17
16. Bruna PJ, Peyerimhoff SD, Buenker RJ (1981) Chem Phys Lett 72: 278
17. Szalay PG, Bartlett RJ (1993) Chem Phys Lett 214: 481
18. Szalay PG, Bartlett RJ (1993) J Chem Phys 103: 3600
19. Gdanitz RJ, Ahlrichs R (1998) Chem Phys Lett 143: 413
20. Szalay PG, Müller T, Lischka H (2000) Phys Chem Chem Phys 2: 2067
21. Widmark PO, Malmqvist PÅ, Roos BO (1990) Theor Chim Acta 77: 291
22. Takagi K, Oka T (1963) J Phys Soc Jpn 18: 1174
23. Andersson K, Fülscher MP, Kalström G, Malmqvist PÅ, Olsen J, Roos BO, Sadlej AJ, Blomberg MRA, Siegbahn PEM, Kellö V, Noga J, Urban M, Widmark PO (1994) Molcas, version 3
24. Lischka H, Shepard R, Shavitt I, Brown FB, Pitzer RM, Ahlrichs R, Böhm HJ, Chang AHH, Comeau DC, Gdanitz R, Dachsel H, Dallos M, Erhard C, Ernzerhof M, Gawboy G, Höchtl P, Irle S, Kedziora G, Kovar T, Müller T, Parasuk V, Pepper M, Scharf P, Schiffer H, Schindler M, Schüler M, Stahlberg E, Szalay PG, Zhao JG (2000)Columbus, an ab initio electronic structure program, release 5.7
25. Shepard R, Shavitt I, Pitzer RM, Comeau DC, Pepper M, Lischka H, Szalay PG, Ahlrichs R, Brown FB, Zhao JG (1988) Int J Quantum Chem S22: 149
26. Lischka H, Shepard R, Pitzer RM, Shavitt I, Dallos M, Müller T, Szalay PG, Seth M, Kedziora GS, Yabushita S, Zhang Z (2001) Phys Chem Chem Phys 3: 664
27. Helgaker T, Jensen HJA, Jørgensen P, Ruud K, Ågren H, Andersen T, Bakken KLBV, Chiristiansen O, Dahle P, Dalskov EK, Enevoldsen T, Heiberg H, Hettema H, Jonsson D, Kirpekar S, Kobayashi R, Koch H, Mikkelsen KV, Norman P, Packer MJ, Saue T, Taylor PR, Vahtras O (1997) Dalton, release 1.0
28. Andersson K, Malmqvist PÅ, Roos BO, Sadlej AJ, Wolinski K (1990) J Phys Chem 94: 5483
29. Müller T, Dallos M, Lischka H (1999) J Chem Phys 110: 7176
30. Price WC (1935) J Chem Phys 3: 256
31. Dallos M, Müller T, Lischka H, Shepard R (2001) J Chem Phys 114: 748
32. Merchán M, Roos BO, McDiarmid R, Xing X (1996) J Chem Phys 104: 1791
33. Tozer DJ, Amos RD, Handy NC, Roos BO, Serrano-Andrés L (1999) Mol Phys 97: 859
34. Walzl KN, Koerting CF, Kuppermann A (1987) J Chem Phys 87: 3796
35. Taylor S, Wilden DG, Comer J (1982) Chem Phys 70: 291
36. Suto M, Wang X, Lee LC (1986) J Chem Phys 85: 4228